THE STUDY OF WAVE PROPAGATION IN A BOREHOLE USING THE FINITE DIFFERENCE METHOD

by

Federico Pardo-Casas, C.H. Cheng and Ralph A. Stephen*

Earth Resources Laboratory
Department of Earth, Atmospheric, and Planetary Sciences
Massachusetts Institute of Technology
Cambridge, MA 02139

ABSTRACT

Synthetic microseismograms of elastic wave propagation in a fluid-filled borehole were generated using both the finite difference technique and the discrete wavenumber summation technique. For the finite difference calculations, the solid-liquid borehole boundary was handled as a sharp boundary using a second order Taylor expansion of the displacements, and additionally, a rigid solid-liquid sharp interface is used to model the existence of the logging tool. A heterogeneous formulation was used to handle variations in formation properties. The finite difference grid has absorbing boundaries on two sides and axes of symmetry on the remaining two sides. A grid size no less than 10 points per wavelength was used. The results from the finite difference modeling were compared with the synthetic microseismograms generated by the discrete wavenumber summation method. A detailed comparison between the microseismograms generated by the two methods showed that the body waves (refracted P and S waves) are identical, while the guided waves showed a slight difference in both phase and amplitude. These differences are believed to be due to the dispersion generated by the finite difference method. We have studied the depth of investigation of the refracted body waves in an invaded or damaged borehole using the conventional ray theory approach and compared the results to those obtained by the finite difference method. The results show that the minimum source-receiver separation necessary to observe the unaltered formation depends on both the velocity gradient and the lowest and highest velocity of the damaged zone. Such an investigation shows us the importance of the length of the logging tool to be able to "see" past the damaged and invaded zone, and thus enables us to measure the true formation properties, as well as to estimate the depth of the damaged or invaded zone.

INTRODUCTION

It has been well established that in order to fully model the complexity of a borehole a general method that allows for continuously varying formation

---

Permanent address: P.O.Box 567, West Falmouth, MA 02574

properties in vertical as well as radial directions is necessary. These variations are the result of borehole washouts, fractures, damaged or invaded zones and thin beds and horizontal bed boundaries. In the case of full waveform acoustic logging, the finite difference method appears to be ideally suited to model the elastic wave propagation in a borehole with complex geometry. As with every other numerical method, finite difference modelling of elastic wave propagation in a borehole has its limitations together with its applications.

This paper outlines the finite difference method as applied to the full waveform acoustic logging problem in some simple situations such as a solid-liquid sharp interface, a solid-liquid sharp interface plus an invaded or damaged zone and the inclusion of a rigid tool. We will first compare finite difference acoustic logs with logs generated by the discrete wavenumber approach (Cheng and Toksöz, 1981) for a simple undamaged borehole with and without a rigid tool in the center. This will provide a useful check on the accuracy of the two methods since they are different ways of solving the same problem and the nature of the numerical approximations in each case is entirely different. We will then apply the finite difference method to a borehole model with a velocity gradient away from the borehole wall in order to simulate an invaded zone surrounding the borehole. The arrival times as a function of source-receiver separations from the finite difference synthetic microseismograms are then compared with those predicted by conventional ray theory.

THE FINITE DIFFERENCE METHOD AS APPLIED TO A CYLINDRICAL BOREHOLE

The wave equation in seismology has been solved by many different approaches. A good review of all the methods appeared in a paper by Chin *et al.* (1982). The principal goal is to calculate synthetic microseismograms that will allow us to better understand the forward problem and to solve the inverse problem. Finite difference and finite element techniques are powerful methods of obtaining synthetic microseismograms for complicated geometries as well as for simpler cases. However, the computation of the high-frequency response becomes expensive because of the need for smaller meshes. They are known to be useful in a case of a laterally heterogeneous medium, because the amount of computation is not necessarily dependent on the geometrical complexity. It is important to note that there is no method which can efficiently and accurately compute the entire frequency response of an inhomogeneous elastic medium to an arbitrary source.

We have chosen the finite difference method to model the elastic wave propagation in a fluid-filled borehole. The main reason for this choice is that the finite difference method is better developed than the finite element method for problems in elastic wave propagation. We used the heterogenous formulation developed by Stephen (1983) and modified by Stephen *et al.* (1983) for our models. The details of the method were given in Stephen *et al.* (1983) and will not be repeated here. We will only highlight the basis for our method to maintain continuity in the discussions.

The equation to be solved is the elastic wave equation for perfectly elastic, isotropic media in the absence of body forces (Aki and Richards, 1980):

$$\rho \ddot{u}_i = \tau_{ij,j} \tag{1}$$

where ρ is density, u_i is the displacement vector and τ_{ij} is the stress tensor for isotropic media, with summation over repeated indices. The stress tensor for isotropic media can be written as

$$\tau_{ij} = [\lambda \delta_{ij} \delta_{kl} + \mu(\delta_{ik}\delta_{jl} + \delta_{il}\delta_{jk})] e_{kl} \tag{2}$$

where λ and μ are Lame's parameters, δ_{ij} is the Kronecker delta, and $e_{kl} = \frac{1}{2}(u_{k,l} + u_{l,k})$ is the strain tensor. Eq. (1) is solved in two-dimensional cylindrical co-ordinates (r,z) and the parameters (ρ,λ,μ) are assumed to be functions of radius r and depth z only. In the case of an open borehole (i.e. borehole without rigid tool), a compressional point source is located in the liquid on the axis of symmetry ($r=0$) and a liquid-solid interface is located at a radius, R. With a rigid tool, a compressional source is located on the wall of the rigid tool and can be viewed as a ring around the tool. A vertical line of pressure receivers will be located below the point source on the axis of symmetry (Figure 1) or along the surface of the rigid tool (Figure 2). The space-time dependence of the source pressure is given in Appendix A2.

It has been shown (Stephen, 1983) that in order to obtain agreement between finite difference and discrete wavenumber results for liquid-solid interfaces, it is necessary to specifically code the boundary conditions for the sharp interface. A second order approximation in the space increments gave the best results. Stephen (1983) compared the results of the finite difference formulation for a sharp liquid-solid interface to the reflectivity method for sea floor models. The second-order formulation for a sharp liquid-solid cylindrical borehole interface was given in Stephen *et al.* (1983). The second-order formulation for a cylindrical rigid tool-liquid interface is given in Appendix A1.

We are also interested in generating synthetic microseismograms in a borehole with an invaded zone. To solve this problem it is necessary to use the heterogeneous formulation of the elastic wave equation. As outlined by Alterman and Loewenthal (1972) and Kelly *et al.* (1976) the elastic wave equation with the parameters (ρ,λ,μ), (functions of radius and/or depth) can be solved directly using an explicit finite difference method. In terms of displacements only, Eqs. (1) and (2) become

$$\rho \ddot{\vec{u}} = (\lambda+\mu)\nabla(\nabla\cdot\vec{u}) + \mu\nabla^2\vec{u} + \nabla\lambda(\nabla\cdot\vec{u}) + \nabla\mu\times(\nabla\times\vec{u}) + 2(\nabla\mu\cdot\nabla)\vec{u} \tag{3}$$

The finite difference formulation of this equation in cylindrical coordinates is given by Stephen (1983). It is necessary to include the density variations because of the sharp density contrast at the borehole wall. The borehole fluid can be taken into account simply by letting the shear modulus, μ, go to zero.

For the case of propagation in infinite homogeneous media, this explicit finite difference formulation is stable only if:

$$\Delta t \leq \frac{\min(\Delta r, \Delta z)}{\sqrt{\alpha^2+\beta^2}} \tag{4}$$

where $\alpha = \sqrt{\frac{\lambda+2\mu}{\rho}}$, $\beta = \sqrt{\frac{\mu}{\rho}}$, Δr and Δz represent the grid size in the radial

and deph axis, and Δt is the timestep necessary to calculate accurately the time derivative.. Kelly *et al.* (1976) suggested that stability in heterogeneous media could be expected provided Eq. (4) held everywhere on the grid. This is only valid for the case of "slowly" varying media. Sharp interfaces treated with the heterogeneous formulation are unstable.

The principal cause of inaccuracy in finite difference calculations for slowly varying media is grid dispersion. If the grid increments ($\Delta r, \Delta z$) are too large, low frequencies will travel faster across the grid than high frequencies causing apparent dispersion. This result is generally true for compressional waves. For shear waves the dispersion relation is more complex and for some combinations of Poisson's ratio and propagation direction high frequencies will travel faster than low frequencies (Bamberger *et al.*, 1980).

Trefethen (1982) found that waves travel faster at 45° and slower along any other direction. An analysis for a general finite difference calculation has been made by Satô and Ishihara (1983), yielding similar results. Compressional waves are slower at high frequencies and shear waves are slower at low frequencies. The dispersion is also dependent on the ratio $\frac{\lambda}{\mu}$; the closer to 1 this ratio is, the smaller the dispersion will be.

Estimates of the number of grid points per wavelength which will give acceptable results vary from ten to thirty and depend on the problem. In particular, in problems where normal modes exist (as in the borehole problem), because of the selective excitation of different modes, great care must be taken in the choice of the proper number of grid points and the proper wavelength to consider. There is no hard and fast rule as to the number of points per wavelength to use in these circumstances. This uncertainty makes the comparison of finite difference results with results of other techniques extremely important.

In order to minimize the computation time for the problem, it is necessary to minimize the size of the grid. This is accomplished by the proper selection of axes of symmetry and absorbing boundaries. If absorbing boundaries are not used (e.g., the displacement is simply set to zero at some distance from the source), the grid dimensions would necessarily be large in order to prevent the reflections from these artificial boundaries from producing interference at the receivers.

In the present model the top and left-hand boundaries are selected to be the axes of symmetry, thus placing the compressional point source in the upper left corner (see Figures 1 and 2). An exact finite difference formulation of the elastic wave equation is possible at axes of symmetry and these are generally preferable to absorbing boundaries where approximations must be made. The axes of symmetry formulation can be obtained from the finite difference formulation by either 1) applying symmetry conditions for the displacements or 2) applying l'Hospital's rule for terms containing $1/r$, (e.g., for the left-hand boundary, $\frac{1}{r}\frac{\partial u}{\partial z}$ becomes $\frac{\partial^2 u}{\partial r \partial z}$ as r goes to zero) (Alterman and Loewenthal, 1972).

For the absorbing boundaries we follow the formulation of Clayton and Engquist (1977), corrected by Fuyuki and Matsumoto (1980) and modified by

Emerman and Stephen (1983), in the right side boundary (r = constant). The method assumes a parabolic approximation to the elastic wave equation about an axis normal to the boundary and works best for energy propagating at near normal incidence. For the lower boundary (z = constant), we follow the formulation of Reynolds (1978). This formulation is more accurate than the previous one in heterogeneous formulation. As with other absorbing boundaries, this method works best for waves propagating at near normal incidence.

Guided waves are not absorbed by boundary conditions based on the parabolic approximation (Fuyuki and Matsumoto, 1980). The elliptical particle motion of the guided waves causes that component of displacement parallel to the boundary to pose problems if the boundary is close to the borehole. A minimum of two wavelengths of the lowest frequency guided wave was used as a criterion for the placement of the grid boundary from the liquid-solid sharp interface to avoid this problem.

APPLICATIONS

In this section we present applications of the finite difference method using an open borehole, with and without a rigid logging tool in the center, with a sharp liquid-solid interface, in a homogeneous formation, and in a formation with a velocity gradient away from the borehole in order to simulate a damaged or invaded zone around the borehole. We will first compare our results in the homogeneous formation with and without a rigid tool to results generated by the discrete wavenumber summation method. We will then present our finite difference results in a damaged or invaded borehole. We will compare the P wave arrival times from the finite difference model with those predicted using ray theory. The models used in these studies are listed in Table 1.

Rigid Tool

Figures 3 and 4 illustrate results from assuming Model 1 (Table 1) in an open hole. Figure 3 is obtained with the finite difference method and Figure 4 is generated with the discrete wavenumber method. The center frequency is 12 kHz, and the bandwidth is 4 kHz.

The different features, P and S wave arrivals, pseudo-Rayleigh and Stoneley waves, are clearly shown in this case. The vertical scale is relative between the different figures. The finite difference method has almost no problems with reflections coming from the absorbing boundaries. The match is good but not perfect. The P and S arrivals show good agreement between the finite difference and the discrete wavenumber results. The pseudo-Rayleigh and Stoneley wave packets show phase and amplitude differences between the two methods. This is probably because of the existence of the second mode of the pseudo-Rayleigh wave affects the grid points per wavelength ratio, as discussed in Stephen *et al.* (1983) in last year's report. The grid dispersion effect induced by the finite difference method also contributes to the differences in the two methods.

Figures 5 and 6 illustrate the case of the inclusion of a rigid tool of 4.5 cm radius (Model 1 Table 1). Note the increased number of reverberations between

the P and the S arrival owing to the smaller water column thickness. In general, the P waveforms in the microseismograms generated with a rigid tool show more beating than those generated in an open borehole with the same borehole radius. This is an expected observation. The match between the two methods is surprisingly good, though again the last parts of the waveforms do no match well. The better match between the two methods than the open borehole case is partly due to the fact that with a smaller fluid annulus in this case, the dispersion curves for the pseudo-Rayleigh wave are pushed to higher frequencies (Cheng and Toksöz, 1981). Thus the second mode of the pseudo-Rayleigh wave is not excited in this case and the number of grid points per wavelength remains relatively constant in the pseudo-Rayleigh wave packet. This shows the importance of the influence of the different modes of the guided waves and the care one must take in the generation of the finite difference synthetics.

Damaged or Invaded Zone

The determination of the elastic properties of a formation with a sonic tool in a borehole is often complicated by the presence of a damaged or invaded zone immediately surrounding the borehole as a result of drilling activity. This zone usually has P and S wave velocities lower than the "virgin" formation. The long spacing full waveform acoustic logs may be able to "see" past this altered zone and measure the true formation velocity. To verify this we have studied the depth of investigation of refracted body waves in an altered borehole using both the ray theory approach and the finite difference method. We first calculate the minimum source-receiver separation necessary to observe the unaltered formation using ray theory. It is clear that it depends on both the velocity gradient and the extent of the altered zone. However, since the wavelength of the elastic waves generated by a full waveform acoustic logging tool is of the order of the borehole radius and/or the thickness of the invaded zone, it is not clear that ray theory works under these circumstances. We therefore generated synthetic microseismograms using the finite difference method with the heterogeneous formulation. We can then compare the results from the two methods.

The velocity characteristics of this problem are presented in Figure 7, and we can observe how the damaged zone is represented. Only the P wave propagation is analyzed here. The model has a liquid-solid sharp interface with a zone of constantly increasing velocity between the interface and the formation. The shaded area represents the possible S wave velocity values that this layer may have.

In order to better understand the phenomenon, a ray tracing of the linear velocity gradient zone is presented (Figure 8). We observe that if the radius of the damaged zone increases, the ability to observe a ray coming back from the formation is reduced due to the larger source-receiver separation necessary to observe that ray. If we increase the velocity gradient without changing the width of the zone, the source-receiver separation necessary to see the ray coming back from the virgin formation is reduced (Figure 9).

We calculate the minimum source-receiver separation that will permit us to observe the properties of the formation through the altered zone using the following equation derived from ray theory:

$$z = 2D\left[\frac{v_1 + v_0}{v_1 - v_0}\right]^{1/2} + 2R\,\frac{v_f}{(v_1^2 - v_f^2)^{1/2}} \qquad (6)$$

where z is the value for the minimum source-receiver separation required to "see" the unaltered formation in an open borehole with an invaded zone of thickness D and with a positive linear velocity gradient. Table 2 shows some values of z as a function of different formation and invaded zone velocities.

Synthetic microseismograms generated with the finite difference method in a borehole with and without a tool and with an invaded or damaged zone surrounding the borehole are presented in Figures 10 and 11 using Model 2 (Table 1). Between the two cases it is easy to identify the absence of a tool in Figure 10 (i.e. the additional beating and the higher amplitude of the P wave train when the tool is present). Compared with the homogeneous formation case in Figure 3 we observe a small delay in the travel time in the damaged zone case (Figure 10) and an increment in the P wave amplitude. This amplitude increase is due to more energy with a ray parameter close to the critical value being channeled through the damaged zone. This phenomenon is well established in conventional seismology.

Figure 11 presents a damaged zone case with a rigid tool (Model 2 Table 1). It is hard to see a big difference between Figure 5 and Figure 11. The main difference is the amplitude increase of the P wave reverberations and also a small amplitude increase in the S and pseudo-Rayleigh waves, but the observations are too close to the source for this difference to be obvious.

The discrete wavenumber method cannot yet be applied to the case of an invaded zone with a velocity gradient, as we have discussed in this section. It is this kind of application that makes the finite difference method a relatively slow but powerful tool in the study of the effect of heterogeneity on the full waveform acoustic logs.

If we compare the theoretical travel time with the arrival time picks made from the finite difference synthetic microseismograms of a 10 *cm* damaged zone (Figure 12, parameters given in Model 3, Table 1), a good agreement between both methods is observed.

Finally, in Figures 13 and 14 we present record sections for Model 2 (Table 1) in an open hole and with the presence of a rigid tool. The size of the damaged zone in this case is 9 *cm*. The minimum source-receiver separation calculated using Eq. (6) gives us a value of 90 *cm* for the open hole case and 85 *cm* for the rigid tool case. In the figures these values can be related to the decrease in amplitudes of the P waves where the transition from the rays being bent back by the velocity gradient and the rays refracted along the unaltered formation occurs.

Additonally, Figures 15 and 16 show the "snapshots" of the two previous record sections. The differences between the cases with and without a rigid tool in an open borehole are clear. The differences in the amplitudes of the body wave are easily observed, and the pseudo-Rayleigh and Stoneley wave trains can also be compared, as we did with the record sections (Figures 13 and 14). The body wave which refracted through the unaltered formation can be easily

identified in both sections by their different incident angle. In this report volume Stephen and Pardo presented some "snapshots" which can be compared with Figures 15 and 16.

CONCLUSIONS

Synthetic microseismograms of the full waveform acoustic log which demonstrate the salient features of observed microseismograms can be generated by the finite difference method using the heterogeneous formulation. The borehole fluid-solid boundary should be handled separately from the general formulation in order to generate stable results. A comparison between the discrete wavenumber method and the finite difference method showed that the latter should be used carefully in the interpretation of the synthetic microseismograms, especially in the case of the guided waves. The use of a heterogeneous formulation in a borehole with a damaged or invaded zone allows us to compare the theoretical travel time arrival with the value obtained from the computed record sections. This comparison illustrates the need for a long logging tool to be able to "see" past the damaged and invaded zone. The inclusion of a rigid tool in the formulation makes the comparison more realistic. This paper shows the power of the finite difference method to solve the wave equation in a heterogeneous medium as opposed to other standard techniques that may need for each case a special formulation which may be difficult if not impossible to obtain. This property makes it possible to easily formulate a varying radius borehole, or a borehole within horizontal bedding, or other heterogeneous borehole environments.

TABLE 1: MODEL PARAMETERS USED IN THIS STUDY

Model 1

V_f = 1.65 km/sec V_p = 4.00 km/sec
V_s = 2.30 km/sec
ρ_f = 1.50 gm/cc ρ = 2.30 gm/cc
R = 9 cm

Model 2

V_f = 1.65 km/sec V_{p0} = 3.63 km/sec V_{p1} = 4.00 km/sec
ρ_f = 1.20 gm/cc V_{s0} = 2.16 km/sec V_{s1} = 2.30 km/sec
ρ_0 = 2.37 gm/cc ρ_1 = 2.30 gm/cc
R = 9 cm D = 9 cm

Model 3

V_f = 1.80 km/sec V_{p0} = 3.00 km/sec V_{p1} = 4.00 km/sec
ρ_f = 1.50 gm/cc V_{s0} = 1.72 km/sec V_{s1} = 2.30 km/sec
ρ_0 = 2.30 gm/cc ρ_1 = 2.30 gm/cc
R = 9 cm

TABLE 2: DEPTH OF INVASION VERSUS DETECTION DISTANCE

v_f km/s	R m	v_0 km/s	D m	v_1 km/s	z m
1.8	0.1	3.0	0.1	4.0	0.63
1.8	0.1	3.5	0.1	4.0	0.88
1.8	0.1	2.5	0.2	4.0	0.93
1.8	0.1	3.0	0.2	4.0	1.16
1.8	0.1	3.5	0.2	4.0	1.65
1.8	0.1	2.5	0.3	4.0	1.35
1.8	0.1	3.0	0.3	4.0	1.69
1.8	0.1	3.5	0.3	4.0	2.43

z is the minimum source-receiver spacing necessary to "see" the formation in a borehole with a positive linear velocity gradient in the invaded zone.

APPENDIX

A1. Second Order Boundary Conditions for a Rigid Tool-Liquid Cylindrical Interface

The formulation for this case, which is analogous to the formulation for the liquid-solid interface presented by Stephen *et al.* (1983) is given below.

The wave equation in the homogeneous rigid tool to the left of the interface (see Figure 1) is:

$$\rho_0 u_{tt}^0-(\lambda_0+\mu_0)(u_{rr}^0+\frac{1}{r}u_r^0-\frac{1}{r^2}u^0)-\mu_0 u_{zz}^0-(\lambda_0+\mu_0)w_{rz}^0=0 \qquad \text{(A1-1)}$$

$$\rho_0 w_{tt}^0-\mu_0(w_{rr}^0+\frac{1}{r}w_r^0)-(\lambda_0+2\mu_0)w_{zz}^0-(\lambda_0+\mu_0)(u_{rz}^0+\frac{1}{r}u_z^0)=0 \qquad \text{(A1-2)}$$

and in the homogeneous liquid to the right of the interface is:

$$\rho_1 u_{tt}^1-\lambda_1(u_{rr}^1+\frac{1}{r}u_r^1-\frac{1}{r^2}u^1)-\lambda_1 w_{rz}^1=0 \qquad \text{(A1-3)}$$

$$\rho_1 w_{tt}^1-\lambda_1(u_{rz}^1+\frac{1}{r}u_z^1)-\lambda_1 w_{zz}^1=0 \qquad \text{(A1-4)}$$

The boundary conditions which must hold at the rigid tool-liquid interface are the continuity of normal stress,

$$(\lambda_0+2\mu_0)u_r^0+\lambda_0(\frac{1}{r}u^0+w_z^0)=\lambda_1(u_r^1+\frac{1}{r}u^1)+\lambda_1 w_z^1, \qquad \text{(A1-5)}$$

vanishing of the tangential stress in the rigid tool,

$$\mu_0(u_z^0+w_r^0)=0, \qquad \text{(A1-6)}$$

vanishing of the normal displacement,

$$u^0=u^1=0, \qquad \text{(A1-7)}$$

and vanishing of the vertical displacement in the rigid tool,

$$w^0=0. \qquad \text{(A1-8)}$$

The superscripts, 0 and 1, refer to values in the rigid tool and liquid respectively. The only unknown in the derivation is the vertical displacement in the liquid at the interface, $w^1(T,n,l)$. The interface is at a radius of $R=T\Delta r$.

Additional relationships required in the derivation are the Taylor expansions:

$$\Delta r u_r^1+\frac{1}{2}\Delta r^2 u_{rr}^1=u^1(T+1,n,l)-u^1(T,n,l) \qquad \text{(A1-9)}$$

Solving eq. A1-3, A1-4 and A1-9 for the vertical displacement in the liquid at the interface one obtains:

$$
\begin{aligned}
w^1(T,n,l+1) = {} & 2w^1(T,n,l) - w^1(T,n,l-1) \\
& + b_1^*[w^1(T,n+1,l) - 2w^1(T,n,l) + w^1(T,n-1,l)] \\
& + b_2^*[u^1(T,n+1,l) - u^1(T,n-1,l)] \\
& + b_3^*[u^1(T+1,n+1,l) - u^1(T,n+1,l) - u^1(T+1,n-1,l) + u^1(T,n-1,l)] \\
& + b_4^*[u^1(T,n+1,l+1) - 2u^1(T,n+1,l) + u^1(T,n+1,l-1) \\
& \quad - u^1(T,n-1,l+1) + 2u^1(T,n-1,l) - u^1(T,n-1,l-1)] \\
& + b_5^*[w^1(T+1,n+1,l) - 2w^1(T+1,n,l) + w^1(T+1,n-1,l) \\
& \quad - w^1(T,n+1,l) + 2w^1(T,n,l) - w^1(T,n-1,l)] \\
& + b_6^*[u^1(T+1,n+1,l) - u^1(T+1,n-1,l) - u^1(T,n+1,l) + u^1(T,n-1,l)]
\end{aligned}
$$

where

$$b_1^* = \left(\frac{\Delta t^2}{\Delta z^2}\right)^2 \frac{\lambda_1}{\rho_1}$$

$$b_2^* = \frac{\Delta t^2}{\Delta r \Delta z} \frac{\lambda_1}{2\rho_1} \left(\frac{1}{T} - \frac{1}{2T^2}\right)$$

$$b_3^* = \frac{\Delta t^2}{\Delta r \Delta z} \frac{\lambda_1}{2\rho_1}$$

$$b_4^* = -\frac{\Delta r}{4\Delta z}$$

$$b_5^* = \frac{\Delta t^2}{\Delta z^2} \frac{\lambda_1}{2\rho_1}$$

$$b_6^* = \frac{\Delta t^2}{\Delta z \Delta r} \frac{\lambda_1}{\rho_1} \frac{1}{4T}$$

It is important to notice the similitude of the b^* coefficients of the rigid tool-liquid interface and the b coefficients of the liquid-solid interface (Stephen ul et al., 1983), and also the complete equation for the vertical displacement in the fluid.

A2. The Source

Two different sources are used in the solution to the wave equation in the borehole case.

a) Point source in the borehole axis (absence of the rigid tool).

The source is a compressional point source in the fluid-filled borehole. The solution to the wave equation for the compressional displacement potential in a homogeneous liquid in cylindrical coordinate (r,z) is:

$$\varphi(r,z,t)=\frac{A}{4\pi\rho\alpha^2 R}g(t-R/\alpha) \tag{A2-1}$$

where $R = (r^2+z^2)^{1/2}$ is the distance between the source and the observation point,
α is the compressional wave velocity in the fluid,
ρ is the density of the fluid, and,
A is a unit constant with dimensions of $(mass \times space \times length^2/time)$.

In our work the source time function is taken to be (Kelly *et al*, 1976)

$$g(t) = -2\xi T e^{-\xi T^2}, \qquad T = t - t_s \tag{A2-2}$$

where ξ is a pulse width parameter and t_s is a time shift parameter.

Since the displacement $\vec{u}$ is the gradient of the potential:

$$\vec{u}(r,z,t) = \begin{bmatrix} \frac{r}{R} \\ \frac{z}{R} \end{bmatrix} \frac{(-A)}{4\pi\rho\alpha^2}\left[\frac{g(t-R/\alpha)}{R^2}+\frac{g'(t-R/\alpha)}{R\alpha}\right] \tag{A2-3}$$

where

$$g'(t) = -2\xi(1-2\xi T^2)e^{-\xi T^2}. \tag{A2-4}$$

Similarly, the solution to the pressure field $(p = \alpha^2\rho\nabla\cdot\vec{u} = \alpha^2\rho\nabla^2\varphi = -\rho\frac{\partial^2\varphi}{\partial t^2})$ is:

$$p(r,x,t) = \frac{-A}{4\pi\alpha^2 R}g''(t-R/\alpha) \tag{A2-5}$$

where

$$g''(t) = 4\xi^2(3T-2\xi T^2)e^{-\xi T^2} \tag{A2-6}$$

and the Fourier Transform is :

$$F[g''(t)] = i\pi^{1/2}\xi^{-1/2}\omega^3 e^{-\omega^2/4\xi}e^{i\omega(t_s+R/\alpha)}. \tag{A2-7}$$

The peak frequency and bandwidth are determined from the pulse width parameter, ξ. For a pressure source, from Eq. (A2-7), the peak frequency is given by

$$f_{peak} = 0.39\sqrt{\xi} \tag{A2-8}$$

with the upper-half-power and the lower-half-power frequencies given by $0.528\xi^{1/2}$ and $0.266\xi^{1/2}$, respectively. The bandwidth, defined by the distance between the two half-power points, is given by $0.262\xi^{1/2}$. In terms of f_{peak} the values of t_s and t_{max} are set to:

$$t_s = -\frac{R_{min}}{\alpha} + \frac{1.46}{f_{peak}} \tag{A2-9}$$

$$t_{max} = t_s + \frac{R_{max}}{\alpha} + \frac{1.46}{f_{peak}} \tag{A2-10}$$

b) Source in the surface of a rigid tool.

In this case a source model was given by White and Zechman (1968), and Bhasavanija (1983) and consists of the product of two functions. The radial displacement at the rigid tool wall is defined by:

$$u_r = f(t).g(z) \tag{A2-11}$$

where $f(t)$ is a Ricker wavelet (Ricker, 1977) in the time domain and $g(z)$ the source strength distribution along the tool wall. The Ricker wavelet is defined as:

$$f(t) = (1 - \frac{2(t-t_0)^2}{\alpha^2})\exp(-\frac{(t-t_0)^2}{\alpha^2}) \tag{A2-12}$$

if $0 < t < 2t_0$ and, $f(t) = 0$ for $t > 2t_0$, where t_0 is the time when the maximum peak occurs, and $\alpha^2 = \frac{4}{\omega_0^2}$ uses the value of ω_0, the peak frequency of the source spectrum. In the case of the $g(z)$ distribution, the following definition is used:

$$g(z) = \frac{1}{2\pi^2 C}\left\{Si\left[C(z-z_0)+\pi\right] - Si\left[c(z-z_0)-\pi\right]\right\} \tag{A2-13}$$

where z_0 is the center of the source and C is 2π divided by the source length. The function Si is defined in Abramowitz and Stegun (1964).

REFERENCES

Abramowitz M. and Stegun I., 1964. Handbook of Mathematical Functions. Dover Publications.

Aki, K. and Richards, P.G. 1980. Quantitative Seismology: Theory and Methods, W.W. Freeman and Company, San Francisco.

Alterman, Z., and Loewenthal, D. 1972. Computer generated microseismograms. In: Methods in Computational Physics, v. 12: Bolt, B.A., Ed., Academic Press, New York, 35-164.

Bamberger, A., Chavent, G. and Lailly, P. 1980. Etudes de schemas numeriques pour les equations de l'elastodynamique lineaire. Rapports de Recherche, *41*, INRIA, B.P. 105, 78150 Le Chesnay, France.

Bhasavanija K. 1983. A Finite Difference Model of an Acoustic Logging Tool: the Borehole in a Horizontally Layered Geologic Medium. Ph D thesis. Colorado School of Mines. Golden, Colorado.

Biot, M.A. 1952. Propagation of elastic waves in a cylindrical bore containing a fluid. J. Appl. Phys., *23*, 997-1005.

Boore, D.M. 1972. Finite difference methods for seismic waves. In: Methods in Computational Physics, v. 11: Bolt, B.A., Ed., Academic Press, New York, 1-37.

Cheng, C.H. and Toksöz, M.N. 1981. Elastic wave propagation in a fluid-filled borehole and synthetic acoustic logs. Geophysics, *46*, 1042-1053.

Chin R.C.Y., Hedstrom G and Thigpen L. 1982. Numerical methods in seismology. submitted for publication to Journal of Computational Physics.

Clayton, R. and Engquist, B. 1977. Absorbing boundary conditions for acoustic and elastic wave equations. Bull. Seism. Soc. Am., *67*, 1529-1540.

Dobrin, M.B., 1976. Introduction to Geophysical Prospecting. New York, McGraw-Hill.

Emerman, S.H. and Stephen, R.A. 1983. Comment on, "Absorbing boundary conditions for acoustic and elastic wave equations," by R. Clayton and B. Engquist. Bull. Seism. Soc. Am. *73*, 661-665.

Fuyuki, M. and Y. Matsumoto 1980. Finite difference analysis of Rayleigh wave scattering at a trench, Bull. Seism. Soc. Am., *67*, 1529-1540.

Kelly, K.R., Ward, R.W., Treitel, S., and Alford, R.M. 1976. Synthetic seismograms: A finite difference approach. Geophysics, *41*, 2-27.

Reynolds A.C., 1978. Boundary conditions for the numerical solution of wave propagation problems. Geophysics, *43*, 1099-1110.

Ricker N.H., 1977. Transient waves in visco-elastic media: Elsevier Scientific Publishing Co., New York.

Satô Y. and Ishihara K. 1983. On the numerical calculation of wave propagation by the finite difference method. Bull. Earthq. Res. Inst., *58*, 163-173.

Stephen, R.A. 1982. Travel-time curves for a simple sea floor model. Marine Geophys. Res., *5*, 315-326.

Stephen, R.A. 1983. A comparison of finite difference and reflectivity seismograms for marine models. Geophys. J.R. Astr. Soc., *72*, 39-57.

Stephen, R.A., F. Pardo-Casas and C.H. Cheng. 1983. Finite difference synthetic acoustic logs. Massachusetts Institute of Technology Full Waveform Acoustic Logging Consortium. Annual Report, Paper 4.

Trefethen L. 1982. Wave Propagation and Stability for Finite Difference Schemes. Ph. D. Thesis. Stanford University. Stanford, California.

Tsang, L. and D. Rader 1979. Numerical evaluation of the transient acoustic waveform due to a point source in a fluid-filled borehole. Geophysics, *44*, 1706-1720.

Ungar, A. and Ilan, A. 1977. Propagation of elastic waves in vertically inhomogeneous media. J. Geophys., *43*, 33-40.

White, J.E. 1962. Elastic waves along a cylindrical bore. Geophysics, *27*, 327-333.

White, J.E. and R.E. Zechman 1968. Computed response of an acoustic logging tool. Geophysics, *33*, 302-310.

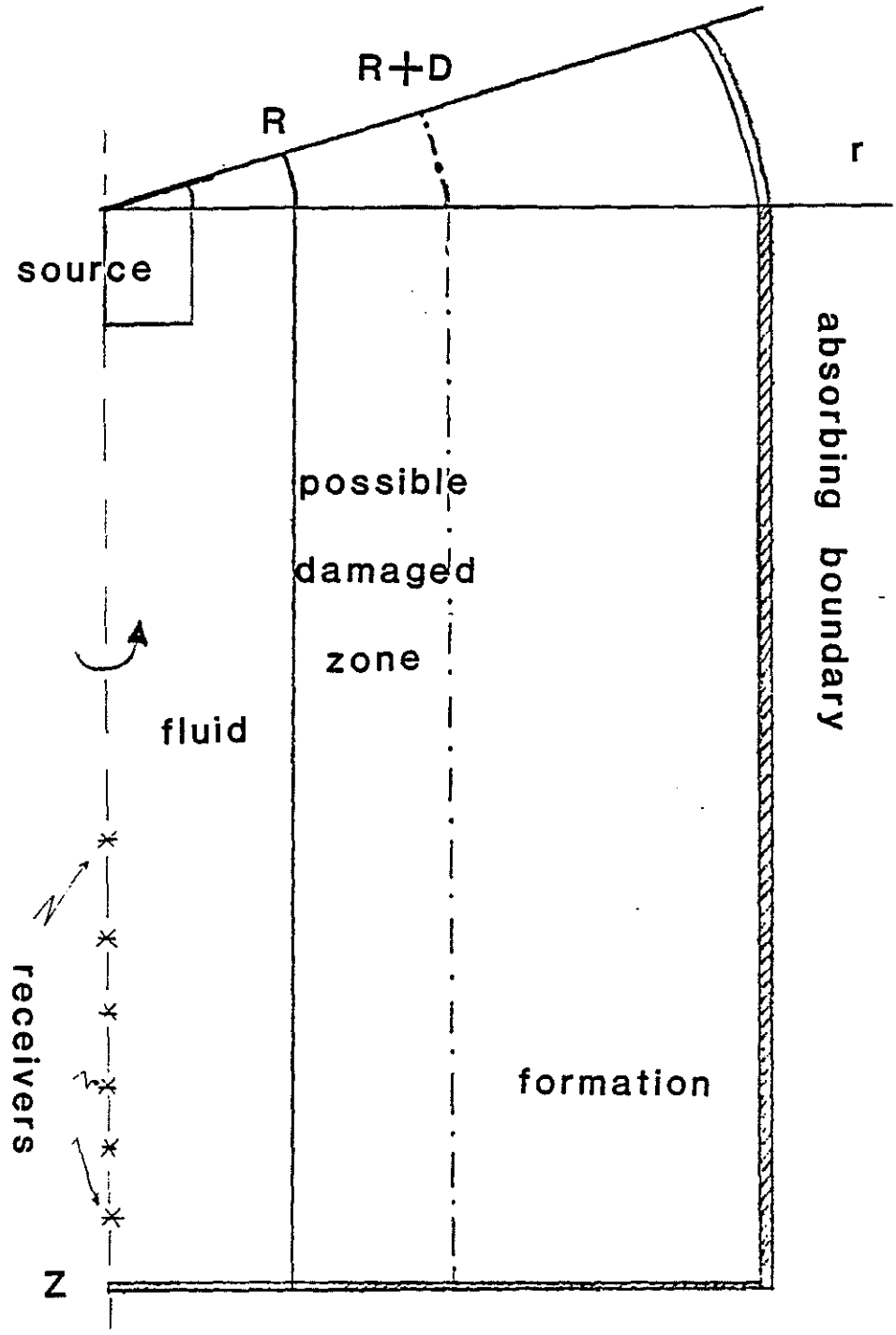

Figure 1. Outline of the geometry used for finite difference synthetic acoustic logs in open hole case. Co-ordinates and types of boundaries are shown.

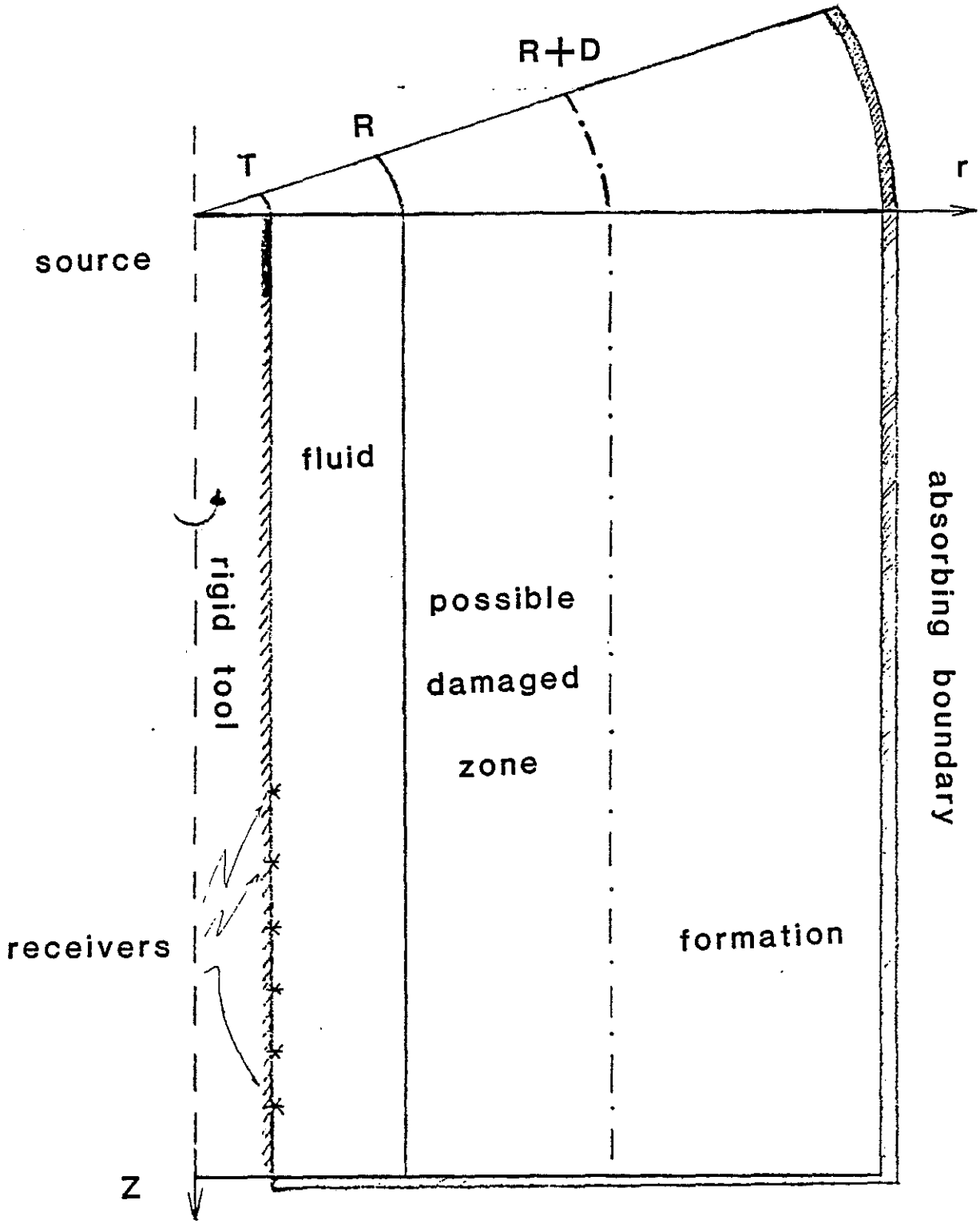

Figure 2. Outline of the geometry used for finite difference synthetic acoustic logs with rigid tool. Co-ordinates and types of boundaries are shown.

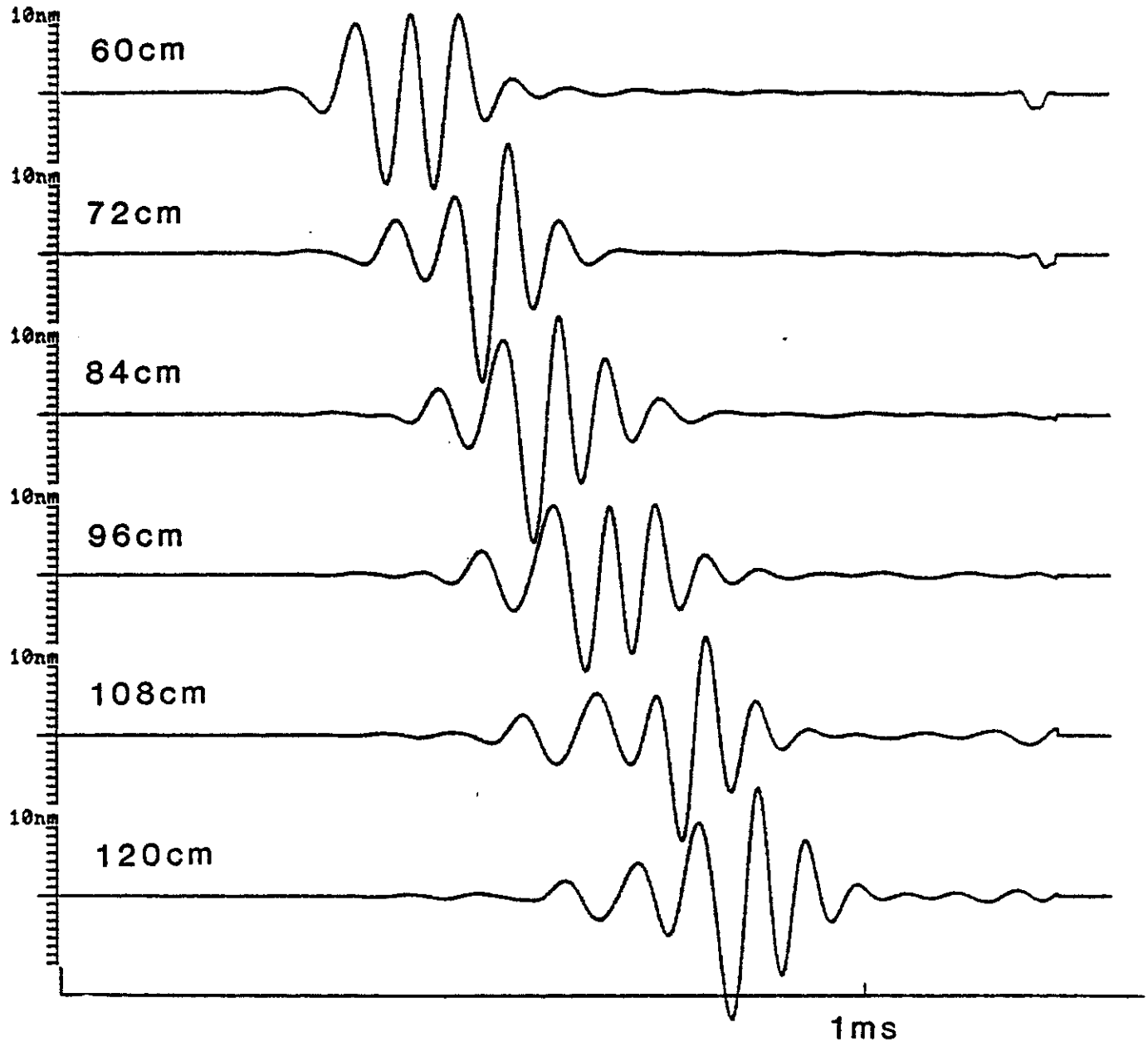

Figure 3. FD synthetic microseismograms using Model 1 in an open hole. The center frequency is 12 *kHz*.

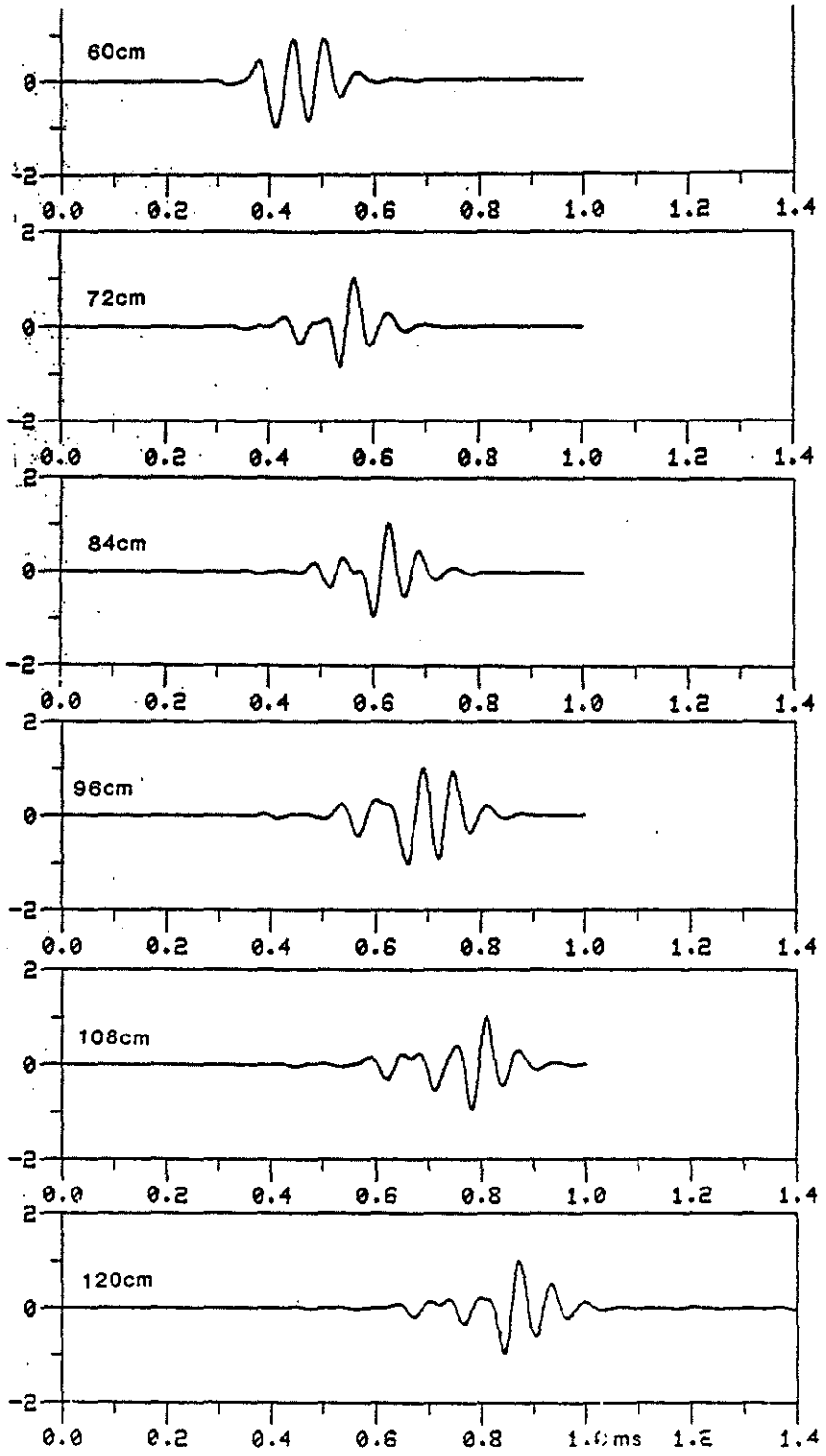

Figure 4. DWN synthetic microseismograms using Model 1 in an open hole. The center frequency is 12 *kHz*.

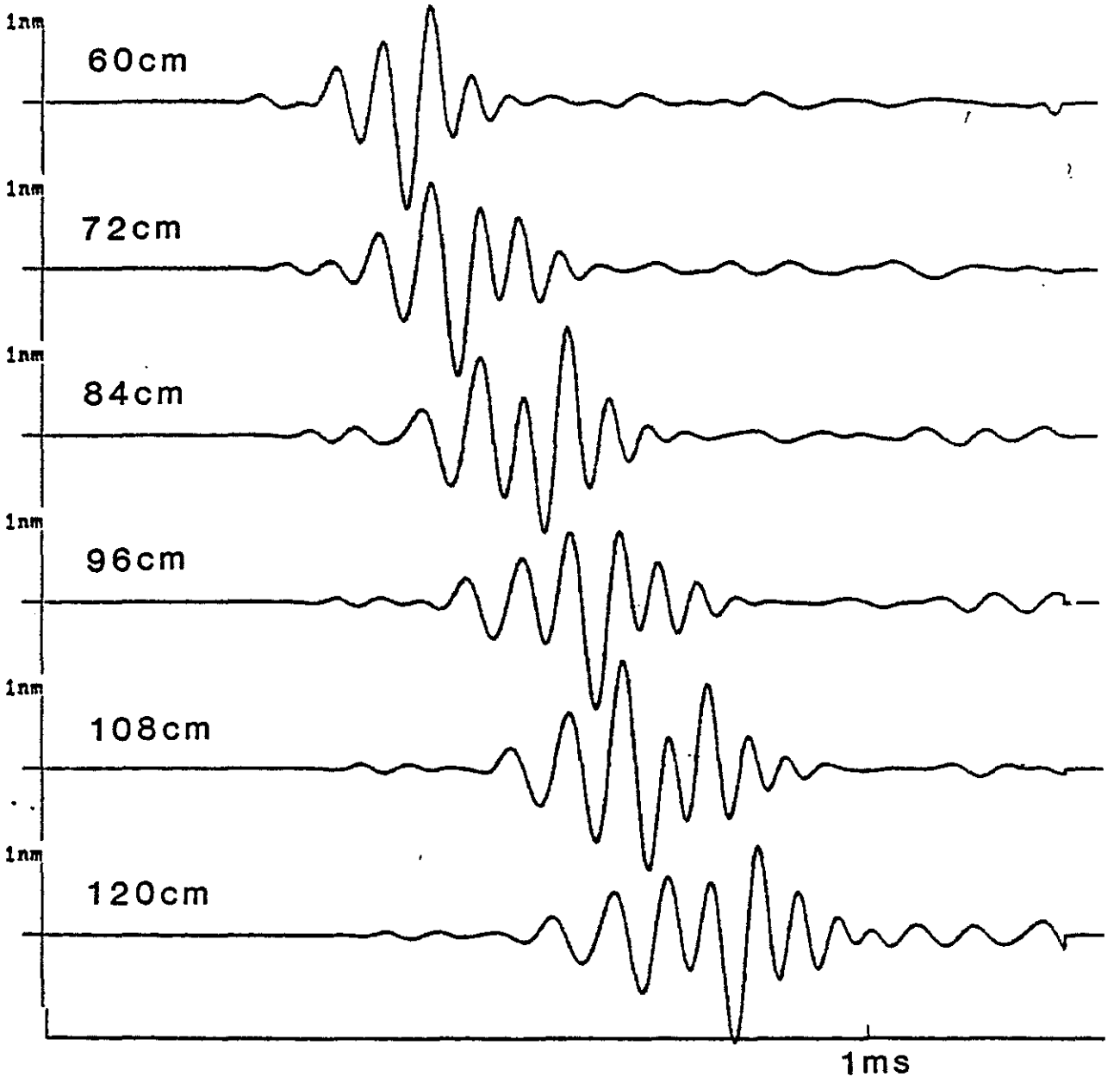

Figure 5. FD synthetic microseismograms using Model 1 and a rigid tool. The center frequency is 12 *kHz*.

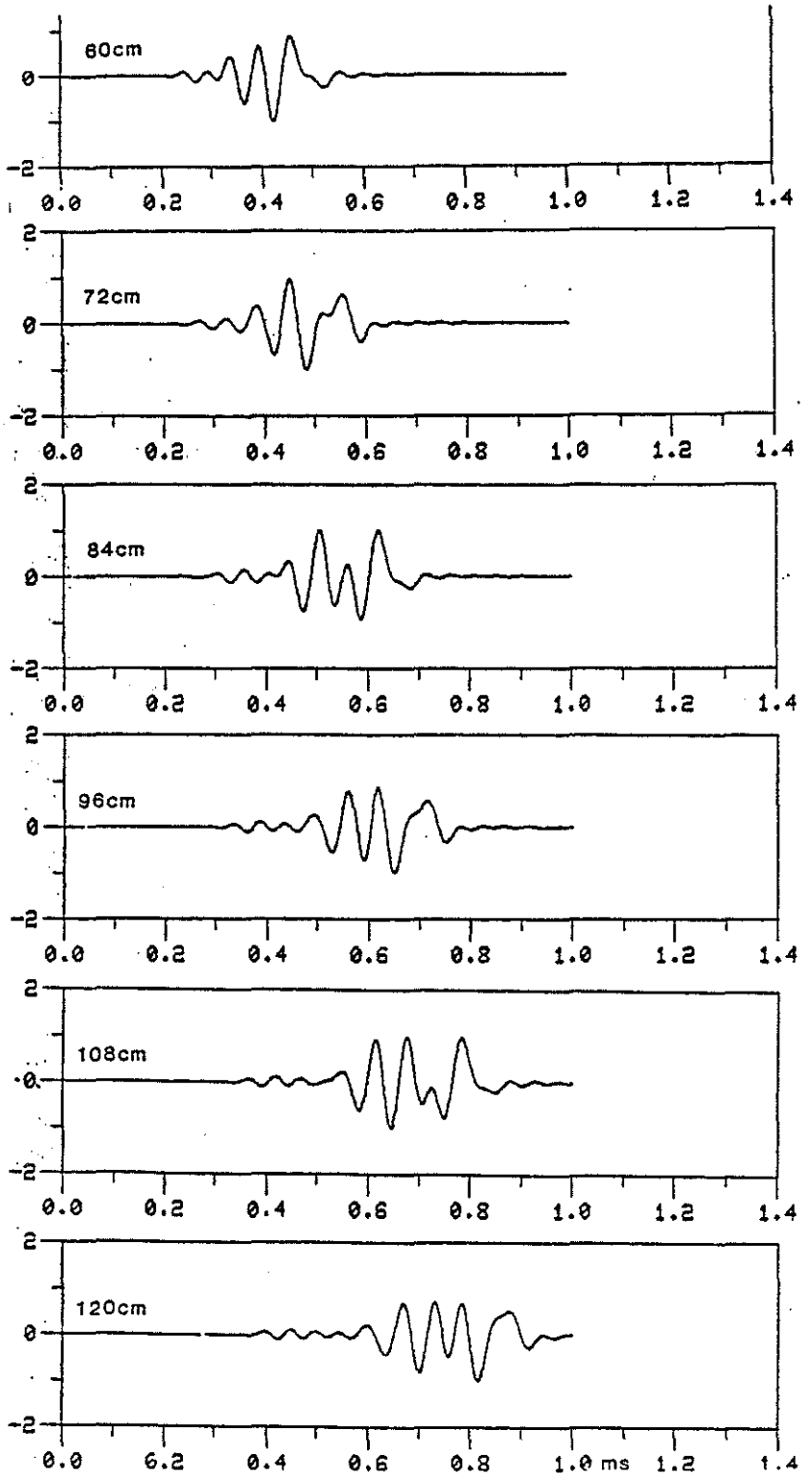

Figure 6. DWN synthetic microseismograms using Model 1 and a rigid tool. The center frequency is 12 *kHz*.

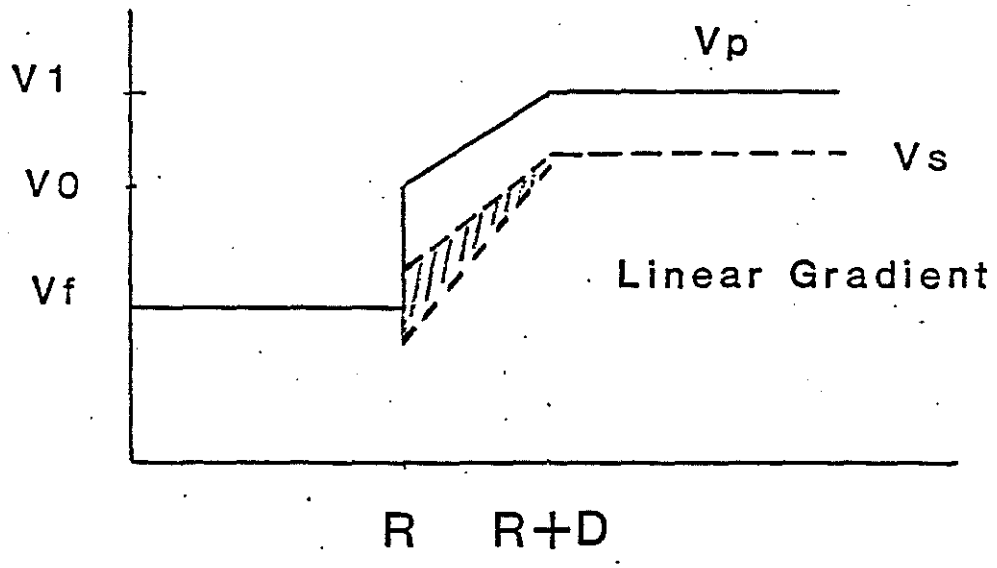

Figure 7. Velocity distribution used in the analysis of the depth of investigation.

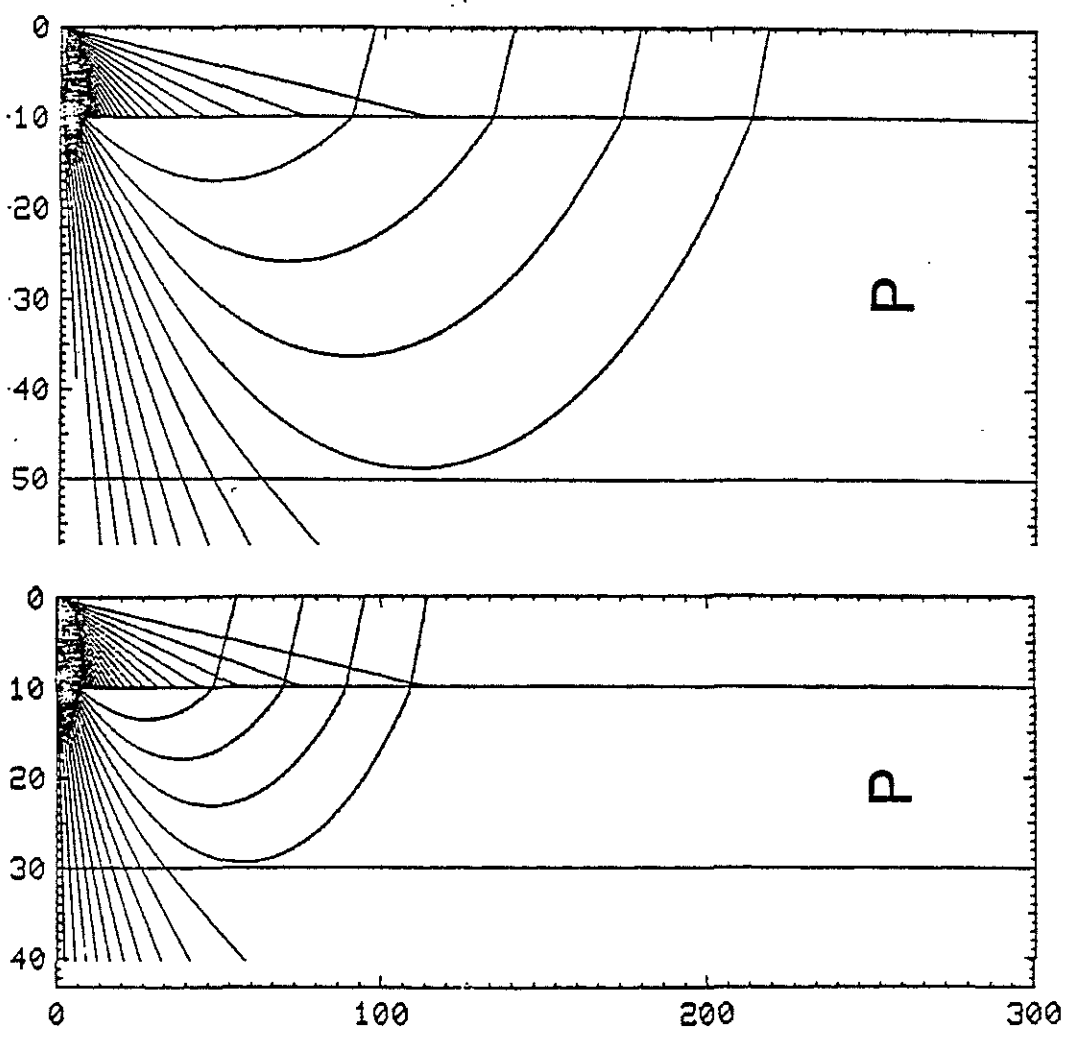

Figure 8. Ray trace in a linear gradient zone. (change of gradient zone size)

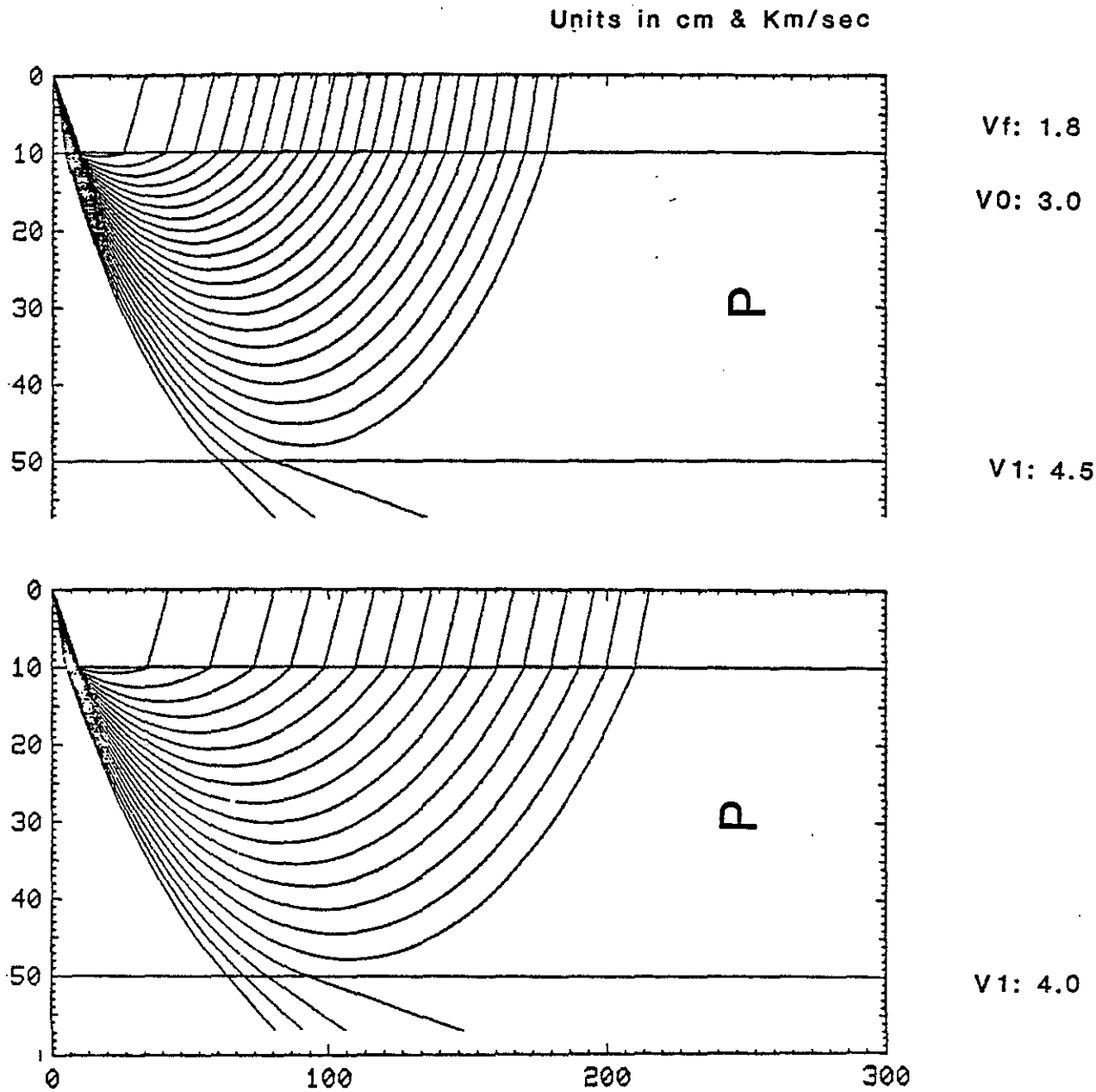

Figure 9. Ray trace of a linear gradient zone. (change of formation velocity)

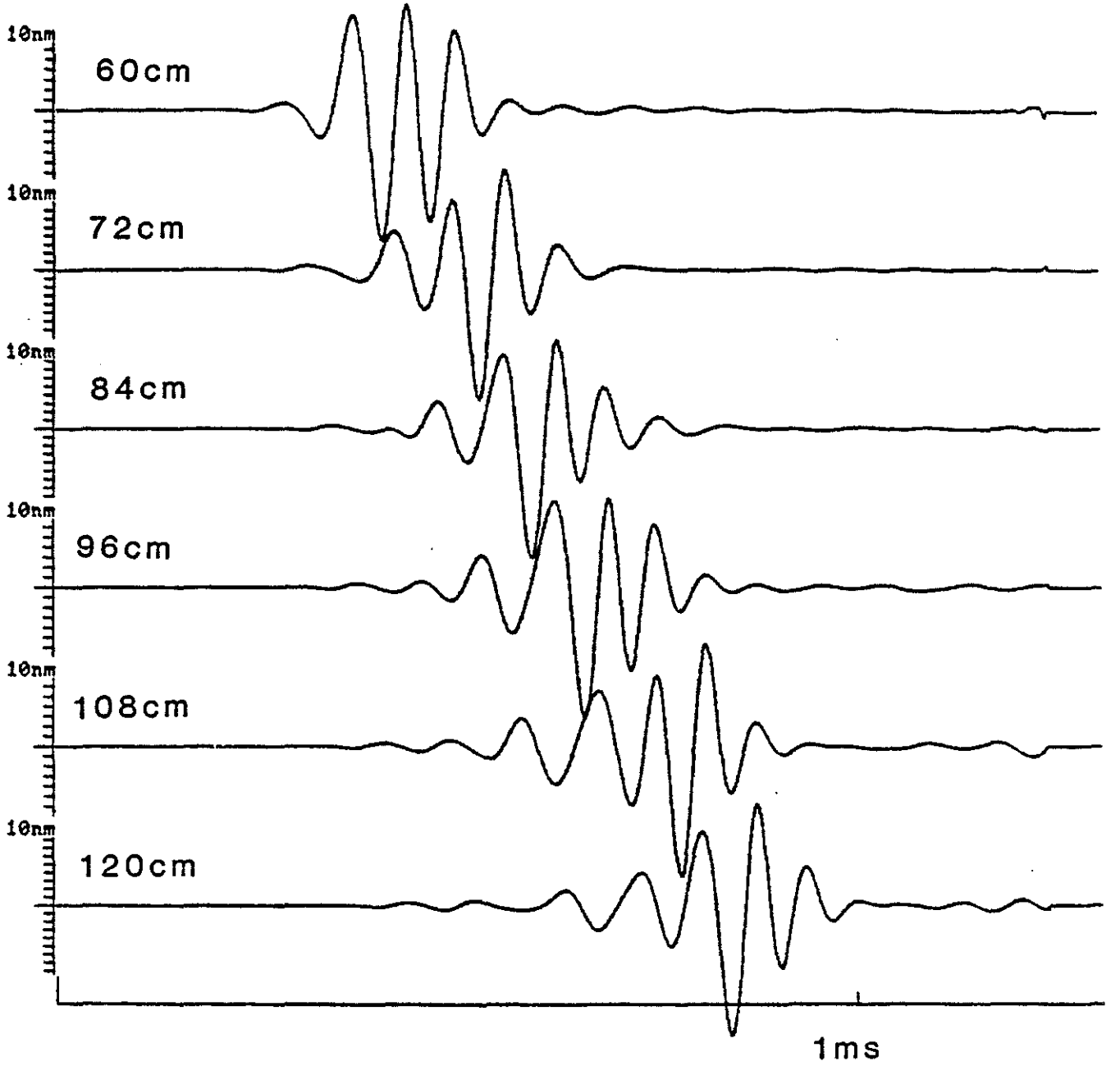

Figure 10. FD synthetic microseismograms using Model 2 in an open hole with a damaged zone.

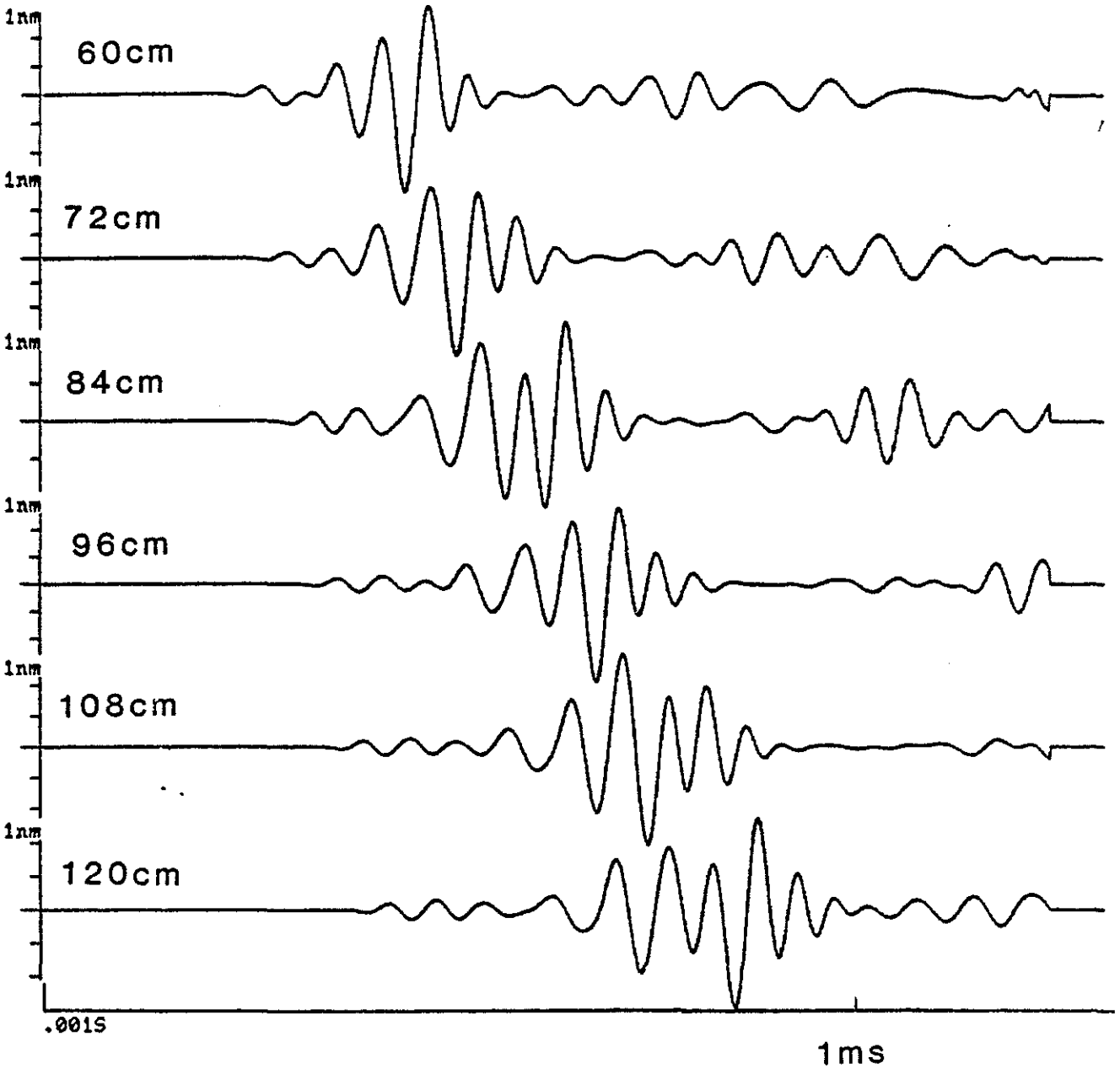

Figure 11. FD synthetic microseismograms using Model 2 in a damaged zone with a rigid tool. The center frequency is 12 *kHz*.

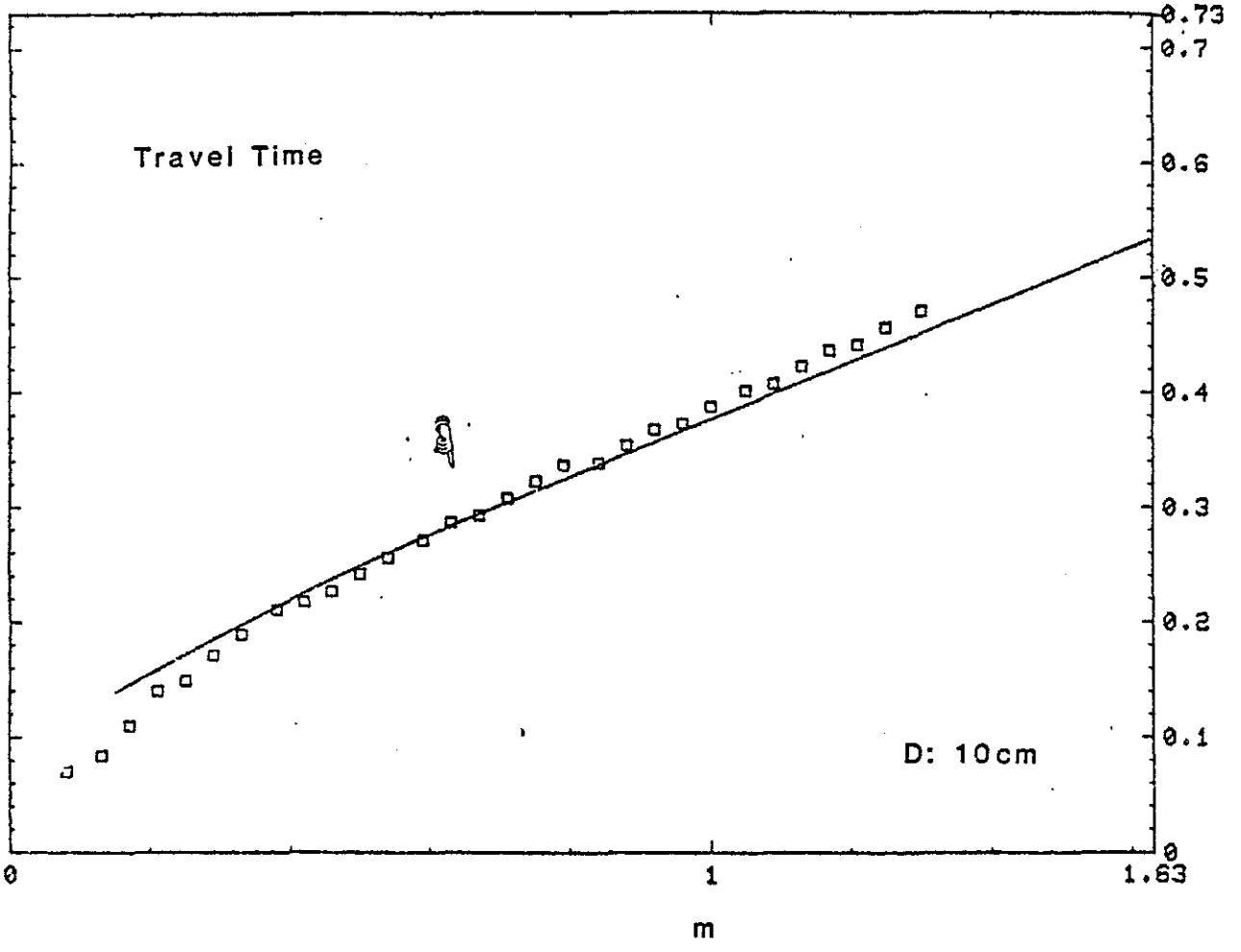

Figure 12. FD synthetic microseismogram travel time picks from case in Model 3 (Table 1) compared with the predicted travel time from ray theory.

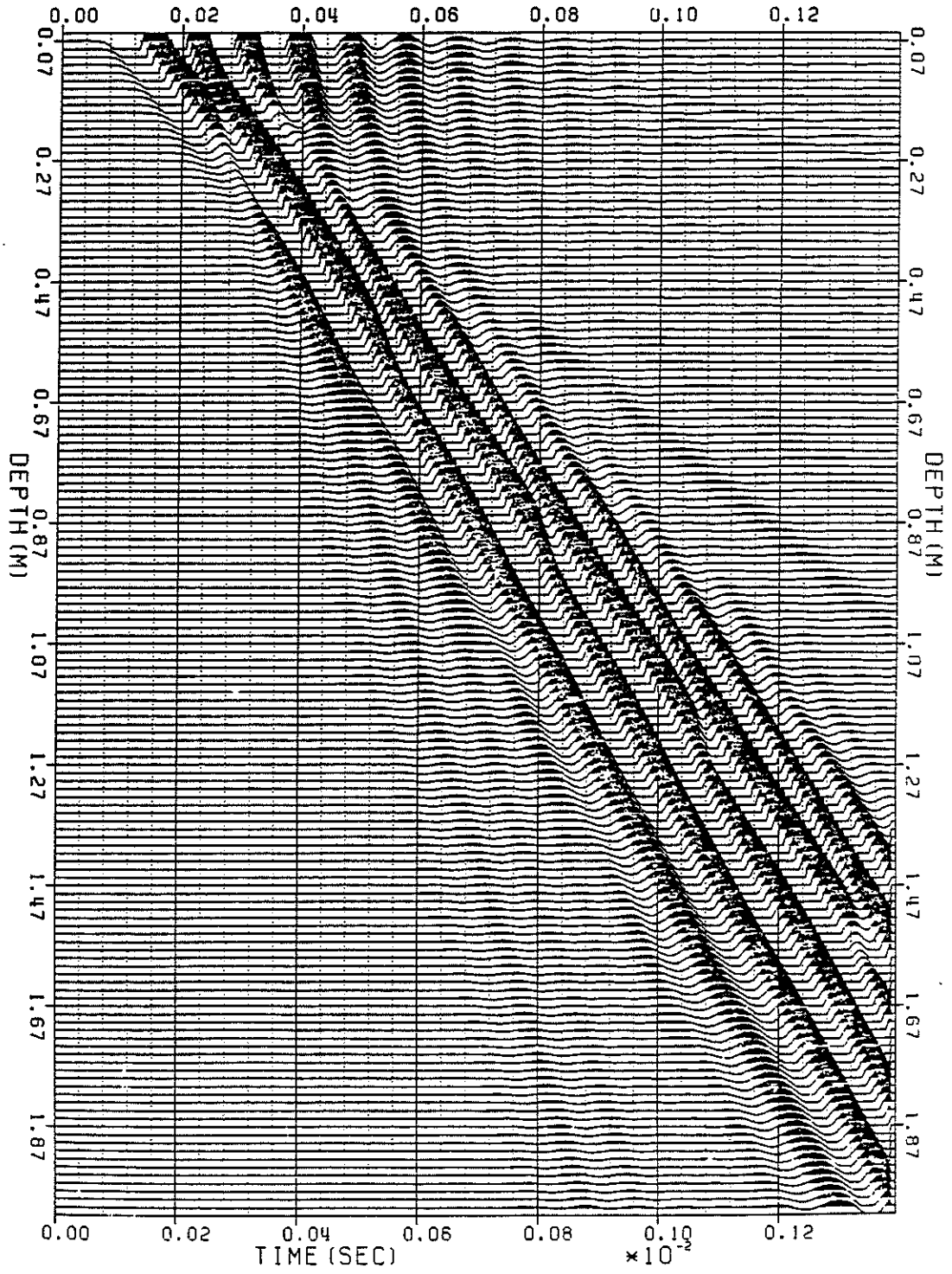

Figure 13. FD synthetic microseismogram using Model 2 in a damaged zone in an open hole.

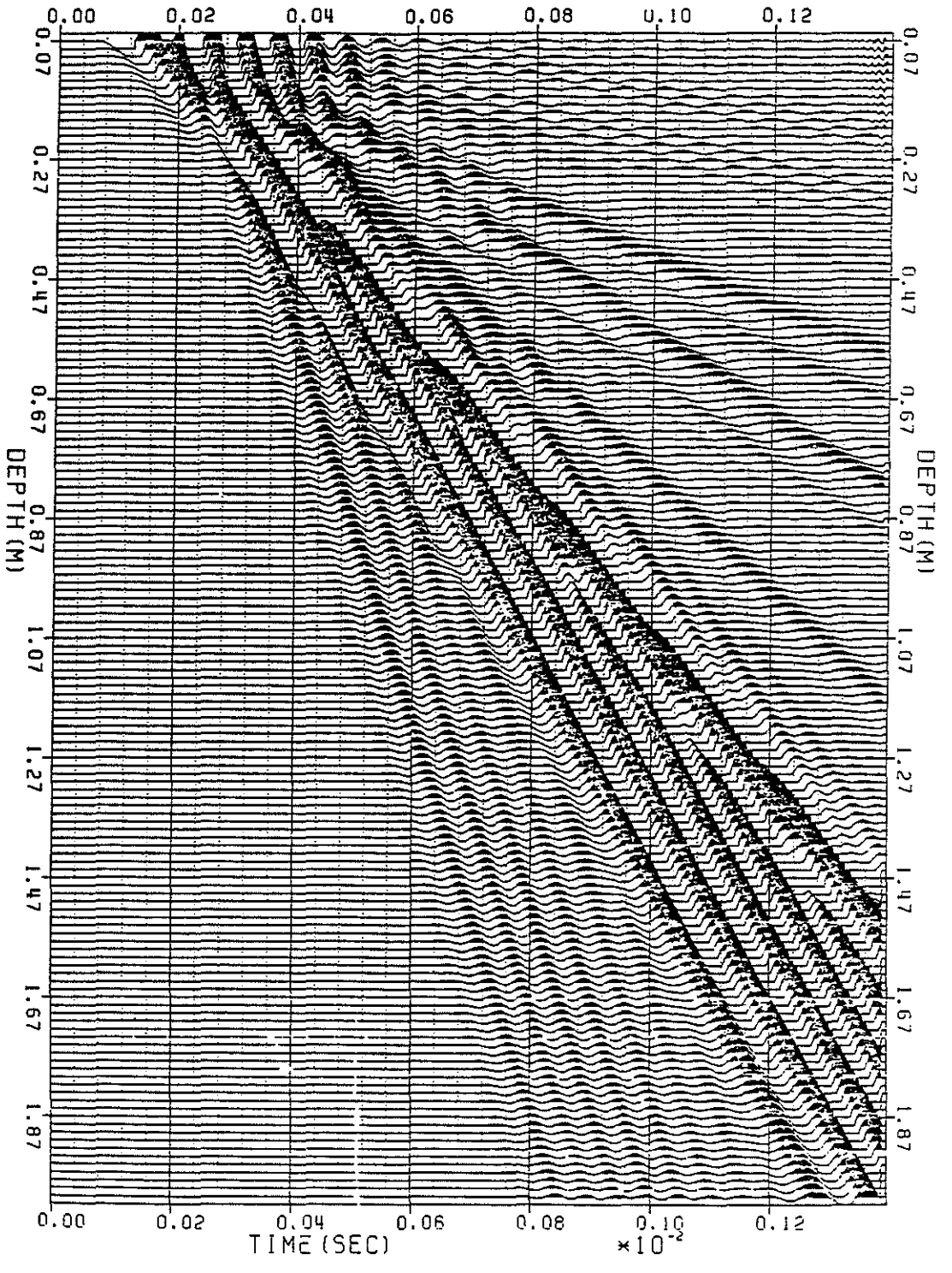

Figure 14. FD synthetic microseismogram using Model 2 in a damaged zone with a rigid tool.

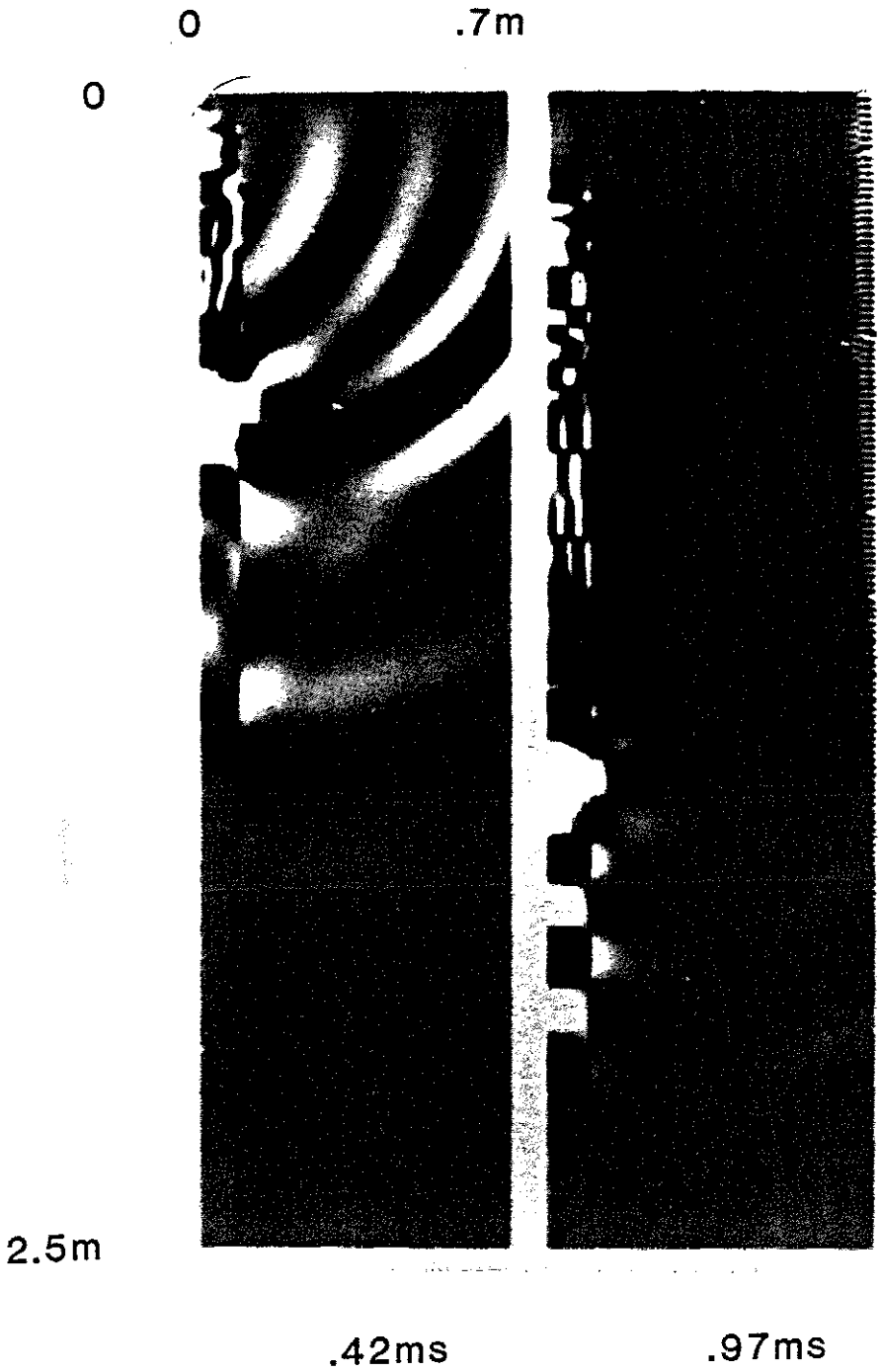

Figure 15. Snapshots of the displacements for the case shown in Figure 13.

Figure 16. Snapshots of the displacements for the case shown in Figure 14.